IETE Technical Review

ISSN: 0256-4602 (Print) 0974-5971 (Online) Journal homepage: http://www.tandfonline.com/loi/titr20

Medical Image Segmentation Methods, Algorithms, and Applications

Alireza Norouzi, Mohd Shafry Mohd Rahim, Ayman Altameem, Tanzila Saba, Abdolvahab Ehsani Rad, Amjad Rehman & Mueen Uddin

To cite this article: Alireza Norouzi, Mohd Shafry Mohd Rahim, Ayman Altameem, Tanzila Saba, Abdolvahab Ehsani Rad, Amjad Rehman & Mueen Uddin (2014) Medical Image Segmentation Methods, Algorithms, and Applications, IETE Technical Review, 31:3, 199-213, DOI: 10.1080/02564602.2014.906861

To link to this article: https://doi.org/10.1080/02564602.2014.906861

Published online: 23 Jun 2014.

Medical Image Segmentation Methods, Algorithms, and Applications

Alireza Norouzi[1], Mohd Shafry Mohd Rahim[1], Ayman Altameem[2], Tanzila Saba[3], Abdolvahab Ehsani Rad[1], Amjad Rehman[4] and Mueen Uddin[5]

[1]Faculty of Computing, Universiti Teknologi Malaysia, Johor, Malaysia, [2]College of Applied Studies and Community Services, King Saud University, Riyadh, KSA, [3]College of Computer and Information Sciences, Prince Sultan University, Riyadh, KSA, [4]MIS Department CBA, Salman bin Abdul Aziz University, Alkharj, KSA, [5]Kulliah of Information and Communication Technology, International Islamic University Malaysia, Kuala Lumpur

ABSTRACT

Medical images have made a great impact on medicine, diagnosis, and treatment. The most important part of image processing is image segmentation. Many image segmentation methods for medical image analysis have been presented in this paper. In this paper, we have described the latest segmentation methods applied in medical image analysis. The advantages and disadvantages of each method are described besides examination of each algorithm with its application in Magnetic Resonance Imaging and Computed Tomography image analysis. Each algorithm is explained separately with its ability and features for the analysis of grey-level images. In order to evaluate the segmentation results, some popular benchmark measurements are presented in the final section.

Keywords:
Image processing, Medical image, Segmentation methods.

1. INTRODUCTION

Medical images have become essential in medical diagnosis and treatment. These images play a substantial role in medical applications because doctors exhibit interest in exploring the internal anatomy [1]. Many techniques have been developed based on X-ray and cross-sectional images like Computed Tomography (CT) or Magnetic Resonance Imaging (MRI), or other tomographic modalities (SPECT, PET, or ultrasound) [2,3].

Over the years, medical image processing has contributed a lot in medical applications; for example, the use of image segmentation, image registration, and image-guided surgery is so common in medical surgery. The oldest one is X-ray which has been applied by the doctors for more than a century. In this technique, electromagnetic radiation with short wavelength and high energy has been used. CT is another medical imaging technique which uses X-ray in imaging internal body organs and structure. It produces a number of parallel slices of each organ by passing X-ray pulses through the body [4–7]. The other imaging technique is Magnetic Resonance Imaging (MRI). It is a developed medical imaging technique that works based on magnetic characteristics and provides a great deal of information about internal organs. This technique has numerous benefits compared to other techniques due to which it is commonly used in medical applications. This technique provides a number of parallel slices for each organ in three dimensions with high contrast between tissues. However, the data volume is too huge for manual analysis, which has been one of the biggest hurdles in MRI application [1,8,9]. Working with MRI has some disadvantages like noise, intensity in homogeneities, low contrast between certain tissues, and partial volume effects in the segmentation task.

The most important part of medical image processing is image segmentation. Image segmentation is a procedure for extracting the region of interest (ROI) through an automatic or semi-automatic process. Many image segmentation methods have been used in medical applications to segment tissues and body organs. Some of the applications consist of border detection in angiograms of coronary, surgical planning, simulation of surgeries, tumor detection and segmentation, brain development study, functional mapping, blood cells automated classification, mass detection in mammograms, image registration, heart segmentation and analysis of cardiac images, etc. [10–18].

In medical research, segmentation can be used in separating different tissues from each other, through extracting and classifying features. One of the efforts is classifying image pixels into anatomical regions which

may be useful in extracting bones, muscles, and blood vessels. For example, the aim of some brain research works is to partition the image into different region colours such as white and different grey spectra which can be useful in identifying the cerebrospinal fluid in brain images, white matter, and grey matter [19]. This process can also prove useful in extracting the specific structure of breast tumors from MRI images [20].

In this paper, we describe several segmentation methods which have been used in recent medical image analysis. Each method will be discussed with its algorithm, advantages, and disadvantages. We classify these methods in four categories: region-based methods, clustering methods, classifier methods, and hybrid methods.

2. REGION-BASED METHODS

A region is composed of some pixels which two by two are neighbours and the boundary is made from differences between two regions. Most of the image segmentation methods are based on region and boundary properties. Here we explain two most popular region-based approaches: thresholding and region growing.

2.1 Thresholding

Thresholding is one of the simplest and fastest segmentation methods based on the assumption that images are formed from regions with different grey levels. The histogram of images has different peaks and valleys which can divide images into different parts [21,22]. Threshold is a value in a histogram that divides intensities into two parts: the first part is the "foreground" having pixels with intensities greater than or equal to the threshold and the second part is the "background" having pixels with intensities less than the threshold [2,23–25]. Therefore,

$$g(x,y) = \begin{cases} \text{foreground if } f(x,y) \geq T \\ \text{background if } f(x,y) \prec T \end{cases} \quad (1)$$

where $f(x, y)$ is the pixel intensity in the (x, y) position and T is the threshold value. An inappropriate threshold value leads to poor segmentation results [26–29]. To separate more than one object with different grey levels, more than one threshold is used which is called multithresholding. Figure 1 shows the application of thresholding in CT images. In this case, thresholding is applied in the CT image of legs to extract the bone area from the background.

Thresholding segmentation usually does not take into account the spatial information of images which leads to sensitivity to noise and intensity in homogeneities.

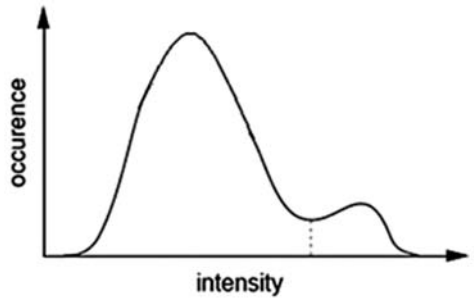

Figure 1: Histogram function with a valley which is useful for the threshold value.

These problems may occur in MRI images which fundamentally destroy the histogram and make partitioning more complex [31–34].

Global thresholding works on the idea that an image has a bimodal histogram and the object can be separated from the background using a threshold value. In the following, local (adaptive) thresholding that uses a local threshold value and Otsu's thresholding that uses an automatic threshold value are described.

2.1.1 Local Thresholding

Global thresholding does not provide satisfactory results for some type of images such as images which do not have a constant background and have diversity across the object. For this kind of images, thresholding provides a good result in one region but fails in other parts of images [25,35]. In order to find different threshold values for different parts of images, the local thresholding method divides images into subimages and then calculates the threshold value for each part. The results of thresholding for each part of an image are then merged. In this method, an image is divided into vertical and horizontal lines, whereas each part includes a region of both the background and the object. Finally, an interpolation is needed to produce appropriate results. Figure 2 shows the application of thresholding in CT images.

Different statistical methods are used to select the threshold value for each subimage, for example, mean, standard deviation, mean and standard deviation together, and mean of maximum and minimum.

Local thresholding needs more time to segment an image compared to global thresholding. This method is more useful in the case of images with varying backgrounds.

2.1.2 Otsu's Thresholding

Threshold value is usually selected visually which leads to problems and may even lead to poor results.

To automate the selection of threshold value, some methods have been presented such as Otsu's method. The goal of Otsu's thresholding is to find an optimal value for global thresholding. In this method, it is assumed that an image has two pixel classes or has a biomodal histogram [36,37]. It chooses the threshold to minimize the intra-class variance (the variance within the class) of black and white cluster pixels.

The intra-class variance could be define using weighted equation of variances of each cluster:

$$\sigma_w^2(t) = q_1(t)\sigma_1^2(t) + q_2(t)\sigma_2^2(t), \tag{2}$$

where the weights q_i are the probability for each class and estimated as

$$q_1(t) = \sum_{i=1}^{t} P(i), \tag{3}$$

$$q_2(t) = \sum_{i=t+1}^{I} P(i), \tag{4}$$

and the class means are given by

$$\mu_1(t) = \sum_{i=1}^{t} \frac{iP(i)}{q_1(t)}, \tag{5}$$

$$\mu_2(t) = \sum_{i=t+1}^{I} \frac{iP(i)}{q_2(t)}. \tag{6}$$

Finally, the individual class variances are given by

$$\sigma_1^2(t) = \sum_{i=1}^{t} [i - \mu_1(t)]^2 \frac{P(i)}{q_1(t)}, \tag{7}$$

$$\sigma_2^2(t) = \sum_{i=t+1}^{I} [i - \mu_2(t)]^2 \frac{P(i)}{q_2(t)}. \tag{8}$$

The process can be stopped here and the algorithm continued by applying the within-class variance for all threshold values t and selecting the value that minimizes $\sigma_w^2(t)$. To achieve faster calculation, we can use the relation between the within-class and between-class variances. Otsu explains that minimizing the intra-class variance is similar to maximizing the between-class variance. After some calculation we have

$$\sigma_b^2(t) = \sigma - \sigma_w^2(t) = q_1(t)q_2(t)[\mu_1(t) - \mu_2(t)]^2. \tag{9}$$

The threshold value that maximizes the between-class variance is the optimal threshold value. Figure 3 shows the application of Otsu's thresholding in cell images.

2.2 Region Growing

Region growing is an interactive segmentation method which requires some seed points to be initialized and start the process. This technique separates a region of images based on some predefined law according to intensity information. In the simplest form, region growing requires one seed point and the region will be grown based on its homogeneity properties according to neighbouring pixels [31,38–41]. There are some region-based methods which have differences in

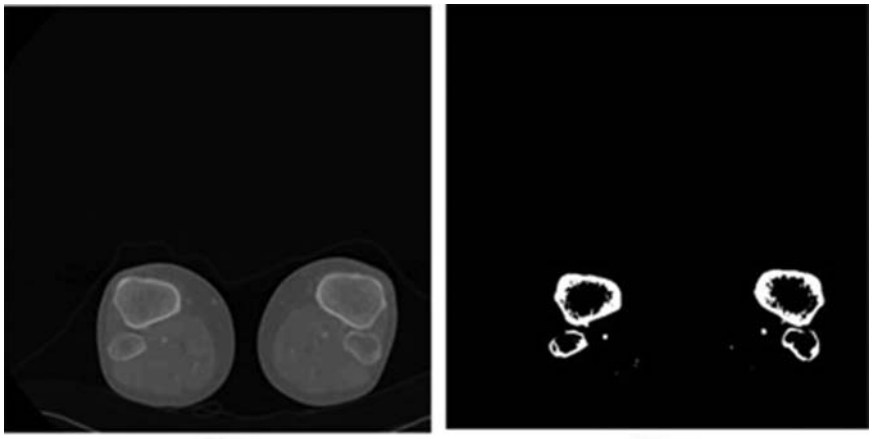

Figure 2: Applying thresholding on the CT image. (a) Original CT images. (b) Extracting the bone by using thresholding segmentation [30].

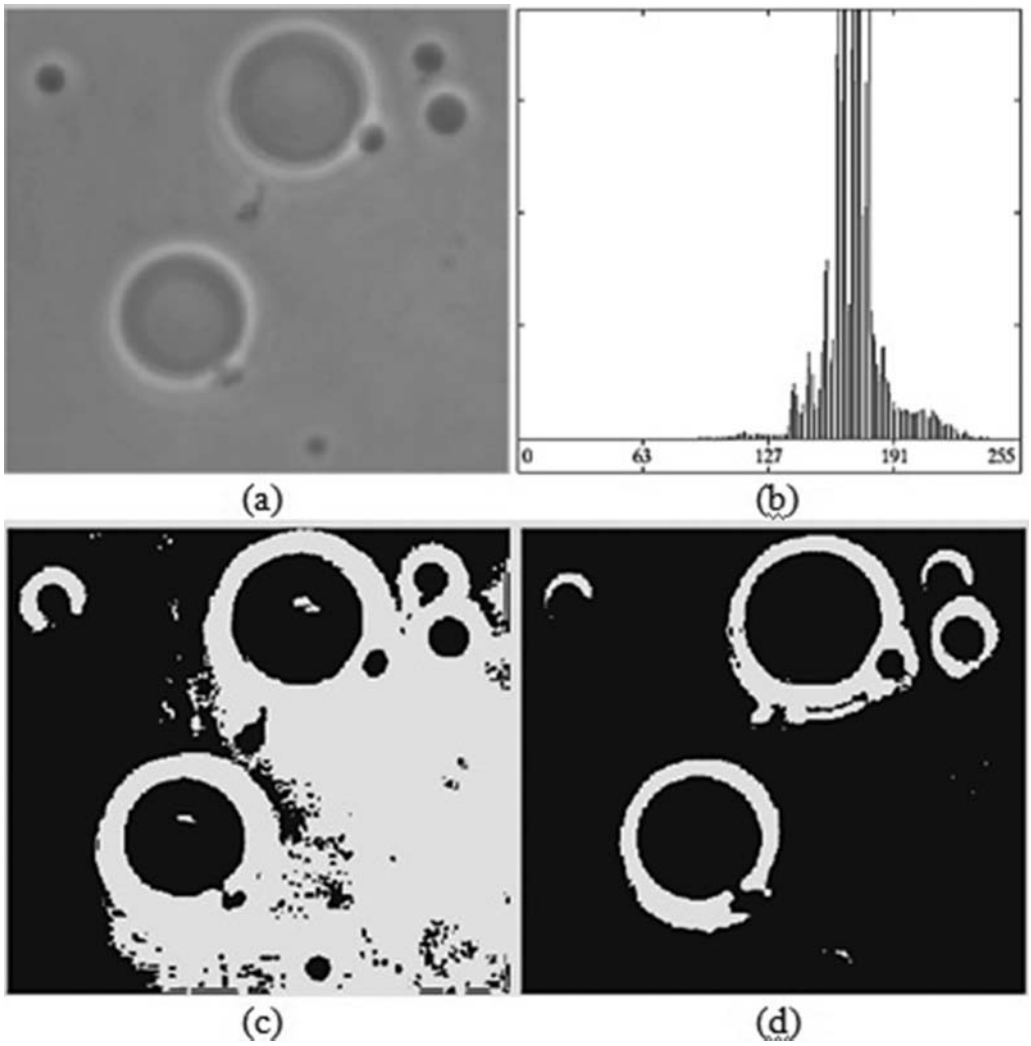

Figure 3: Otsu's thresholding. (a) Original image. (b) Histogram of an image. (c) Global thresholding. (d) Otsu's thresholding.

homogeneity criterion definition. A general region algorithm for extracting one object is as given below:

Algorithm: Input (seed point)

(1) Region $r = \{\text{seed}\}$
(2) While r.neighbours $\neq \{\}$
   (a) For each voxel x in r.neighbours, if $P(x,r) =$ true, then add x to r
   (b) End while
(3) Return r

In the above algorithm, r is a region that we want to extract. Based on homogeneity criteria, some region-growing-based methods have been presented. In this algorithm, the fundamental region-growing method has been explained by evaluating the distance between voxel x and the mean of region which is presented by the function P [42–44]. P is expressed as

$$P(x, r) = |f(x) - \mu_r| < T, \tag{10}$$

where μ_r is the region's mean of r and T is a threshold. The threshold can be selected manually or using an automated method.

In Figure 4, region growing has been applied on the MRI image of the knee. In this figure, two seed points have been selected from two different regions and the region-growing process has been applied.

The disadvantage of region growing is that the result of this technique significantly depends on the seed point selection. Selecting a seed point depends on human ability; thus, the extracted shape considerably

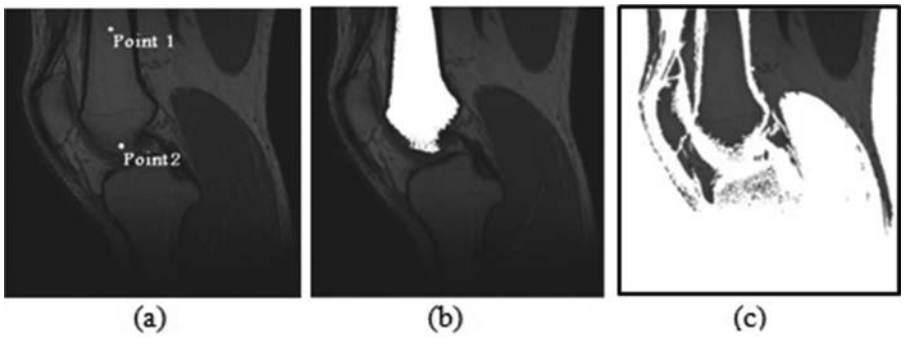

Figure 4: Performing region growing on an MRI bone image. (a) Original images with two seed points. (b) Region growing result for seed point 1. (c) Region growing result for seed point 2.

depends on the user. Although noise sensitivity in this method is less than thresholding, but it can make a hole in the extracted shape or produce a disconnected area [45–48]. Region growing has been widely used in mammograms in order to extract the potential lesion from its background [49].

3. CLASSIFICATION METHODS

Searching for patterns in data, called pattern recognition, is a basic problem with a long history. Classification is a pattern recognition technique which uses training data to find the patterns. Training data includes a sample of image features with their target labels. This technique is known as the supervised learning technique, because it involves training data which are segmented manually and then presented to the automatic process [50–52]. A number of classifier methods have been used for image processing. In this section, we explain two classifiers which are widely used: *k*-nearest-neighbour and maximum likelihood. *k*-nearest neighbour is a simple classifier method and maximum likelihood is a popular parametric classifier method.

The disadvantage of these methods is that they do not take into consideration the spatial information [31,53,54]. Another problem is training data which have to be segmented through human interaction. Segmentation of sample data not only takes more time, but also depends on human abilities.

3.1 *k*-Nearest Neighbour

k-nearest-neighbour (*k-nn*) is a regular non-parametric and commonly used classification method. This method is known as a non-parametric method because the *k-nn* algorithm does not need any information about statistical properties of pixels. The *k-nn* algorithm needs a great amount of sample data which are labelled as training data. Figure 5 explains the idea of this method without using formulae. As shown in the figure, each pixel is classified according to the number of nearest neighbours which are classified before as training data [55–57]. In this algorithm, k is the number of nearest neighbours. To classify new data (Figure 5) with $k = 4$, it should find four nearest neighbours. This set include three data from class 2 and one data from class 1. Thus new data is classified as class 2. To classify new data with $k = 9$, new data with same rule is classified in class 2.

Below, we explain the *k-nn* algorithm.

Algorithm:

(1) Set labelled training data $X_D = \{x_1, \ldots, x_{n_D}\}$ where $X_D \in M_{func}$.
(2) Choose k neighbours to find.
(3) Choose $d : R^p * R^p \rightarrow R^+$ any metric (distance measure) on R^p.
(4) For any vector z in R^p: using $X_D = \{x_i\}$

Calculate and sort the distances $d(z, x_i)$ as $\{d_1 \leq d_2 \leq \cdots \leq d_k \leq d_{k+1} \leq \cdots \leq d_{nD}\}$.

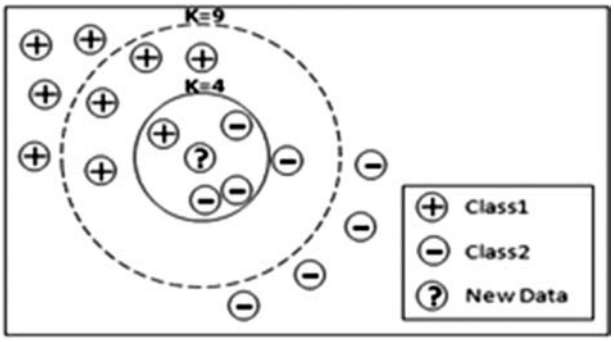

Figure 5: *k*-nearest neighbour illustration.

Find the column in U_d corresponding to the k-nearest neighbour indices {1,2, ... ,k}.

Compute the label vector $U(*|z) = (u(1|z),\ u(2|z),\ \ldots,\ u(c|z))^T$ with k-nn labels from U_d:

$$u(i|z) = \sum_{j=1}^{k} \frac{u_{D,ij}}{k} \quad for\ i = 1, 2,\ \ \ldots, c$$

Decide $x \in i \Leftrightarrow D_{nn,k}(z) = e_i \Leftrightarrow u(i|z) = \max\{u(i|z)\}$,

where z is the new data, X_D is the training data, R^p is the domain, and p is the dimension of data. The term d is the Euclidean distance between two vectors in R^p and is declared as follows:

$$d(z, x_i) = ||z, x_i|| = \sqrt{(z, x_i)^T (z, x_i)}.$$

Here we present the standard k-nn. Three parameters which affect the k-nn results are as follows: (1) finding a suitable k to classify the data, (2) selecting the measurement for distance (like Euclidean distance), and (3) the method of counting votes [58−60].

A fuzzy rule has been applied on k-nn and a new algorithm implemented. In fuzzy k-nn, each datum belongs to a class with some weights [61].

3.2 Maximum Likelihood

Maximum likelihood estimates the parameter of a statistical model. In this method, it is supposed that there is a huge volume of data and we just have a sample set of these data. Finding the distribution of original data is not possible or the cost of it is not reasonable. Thus, we need to find a distribution parameter based on existing data. One of the popularly used distributions is Gaussian distribution. Therefore, we can find the mean and variance of sample data and use it to estimate the original data model. This method tries to find the best estimation for sample data to produce a nearest data model to original data [50,59,62−64].

One of the advantages of this technique is it can be used in a wide range of estimation situations. For example, it can be performed on each sample of original data with various censoring models. The other advantage is approximation of normal distributions and approximation of sample variances that can be applied to produce confidence bounds and suggestion tests for the parameters. One of the disadvantages of this method is that maximum likelihood estimation cannot be applied with small samples of data. Using maximum likelihood estimation with small training data leads to insignificant results. The other advantage is that maximum likelihood can be sensitive to the starting value selection [65−67].

4. CLUSTERING METHODS

The operation of clustering algorithms is like a classification technique with the only difference that clustering algorithms do not need training data. These algorithms are known as unsupervised learning methods. These algorithms work like density estimation in statistics which means that an unsupervised learning algorithm tries to summarize and present data by their main features. Many data mining algorithms have been used in clustering. In this section, we explain three popular clustering algorithms: k-means, fuzzy C-mean, and expectation maximization. Regarding unsupervised methods that do not use learning data, they do not need more time to prepare segmented sample data. One of the advantages of these methods is that they consume less time. As a disadvantage, we cannot refer to spatial information. Like the classification approach, these algorithms do not take note of the spatial information; thus, they can be sensitive to noise and intensity in homogeneities [58,68−72].

4.1 *k*-means

k-means is a widely used unsupervised method which partitions the image into k sections based on the mean of each section. First, data are divided into k clusters and then the mean for each cluster will be calculated [28,43,62]. Each datum is put in the cluster which has the nearest distance to the mean of clusters using the Euclidean distance. The input data is a vector and the output is a k vector. In order to apply k-means on MRI images which are two dimensional, pixels should be put in one vector.

Algorithm: Input (k, data)

(1) Choose k random positions in the input space
(2) Assign the cluster centres μ_j to those positions
(3) For each $x_i \in$ data
  (a) Compute the distance Dist(x_i, μ_j) for each μ_j
  (b) Assign x_i to the cluster with the minimum distance
(4) For each μ_j:

Move the position of μ_j to the mean of the points in that cluster:

$$\mu_j = \frac{1}{N_j} \sum_{i=1}^{N_j} x_i,$$

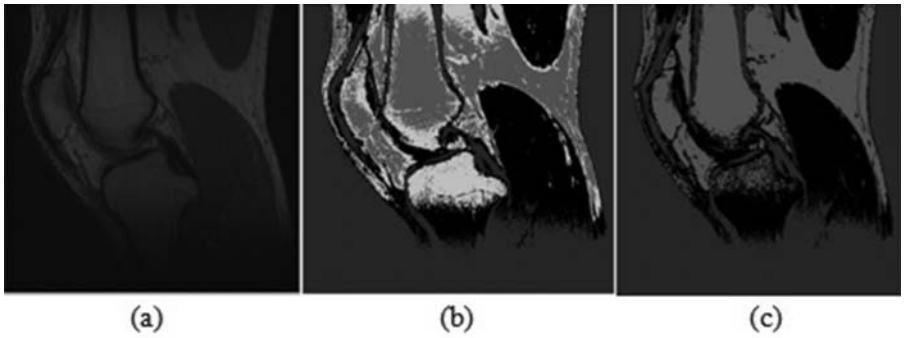

Figure 6: Performing *k*-means on the MRI of the knee bone. (a) Original image. (b) Performing *k*-means with $k = 4$. (c) Performing *k*-means with $k = 3$.

where k is the number of clusters, N_j is the number of data in a cluster j, and μ_j is the mean of cluster j and some of square errors which determine the condition of the repeat loop as

$$\text{SSE} = \sum_{j=1}^{k} \sum_{i=1}^{n} \text{dist}(x_i, c_j)^2.$$

Figure 6 shows the result of applying k-means on MR image of the knee bone.

One of the disadvantages of this algorithm is the number of clusters. User should select the k value to segment the image. Another problem is sensitivity to outliers, noises, and initial values. The initial values are selected randomly from the data vector. Some refinements have been done on this algorithm to improve the problem and an enhanced algorithm has been presented [73–77].

4.2 Fuzzy C-mean

Fuzzy C-mean (FCM) clustering is an unsupervised algorithm which has been performed successfully on medical images. This technique is based on the mean of each cluster and grouping similar data values in the same clusters.

Overlapping usually exists in many grey-scale medical images for different tissues. FCM is one of the suitable clustering methods for medical image segmentation. Several FCM clustering applications have been presented for MRI segmentation of different parts of body [78–81].

Let $X = \{x_1, \ldots, x_n\}$ be a data set where $x_i \in R^d$ and assume there are k clusters and c_j is the centroid of cluster j. Then, we have

$$c_1, c_2, \ldots, c_k \; k \text{ clusters}, \; c_j : j = 1, \ldots, k.$$

Let w be a weight matrix where each value belongs to each cluster with a specific value.

$$w = \begin{bmatrix} w_{1,1} & w_{n,1} \\ w_{1,k} & w_{n,k} \end{bmatrix}, w_{i,j} \in [0, 1]. \tag{11}$$

This method has the following two restrictions:

$$\begin{aligned} &1. \textstyle\sum_{j=1}^{k} w_{i,j} = 1 \; \forall x_i \\ &2. \; 0 < \textstyle\sum_{j=1}^{n} w_{i,j} < 1 \end{aligned} \tag{12}$$

We have provided some preliminary information about FCM. Given below is an explanation of the FCM algorithm.

Algorithm:

(1) Initialize a fuzzy partition and set the weight W (for all W_{ij})
(2) Repeat
  (a) Calculate the centre of clusters using the fuzzy partition.
  (b) Update the fuzzy partition, i.e., W_{ij}.
(3) Until the centres do not change.

In this algorithm, c_j is

$$c_j = \frac{\sum_{i=1}^{n} w_{ij}^p . x_i}{\sum_{i=1}^{n} w_{ij}^p},$$

which is an extended edition of the centroid formula which is used in k-means. The difference is just the degree of membership for each pint belonging to e ach cluster [82–84]. Weights are defined as

$$w_{ij} = \frac{(1/(\text{dist}(x_i, c_j)^2)^{\frac{1}{1-p}}}{\sum_{j=1}^{k} (1/(\text{dist}(x_i, c_j)^2)^{\frac{1}{1-p}}}. \tag{13}$$

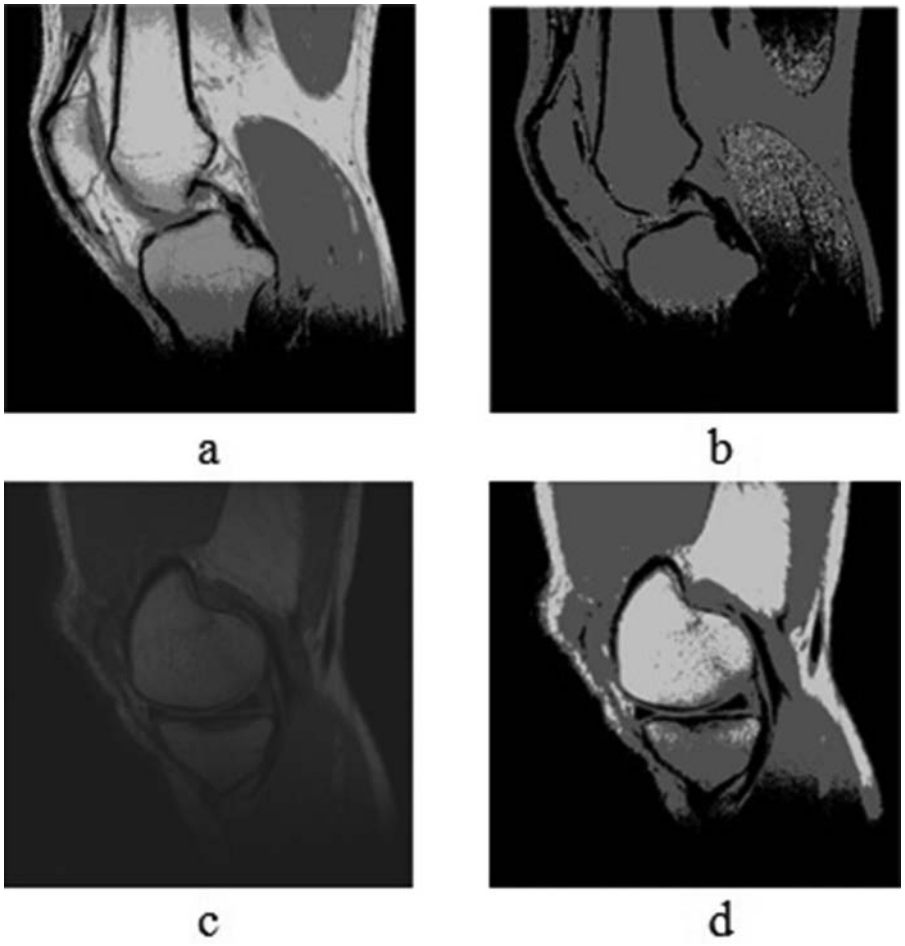

Figure 7: Using FCM with different parameters. (a) Performing FCM with $p = 1.5$. (b) Performing FCM with $p = 10$. (c) Original slice image. (d) Performing FCM with $p = 4$ and three colours.

Some of square errors which determine the condition of repeat loop is

$$\text{SSE} = \sum_{j=1}^{k} \sum_{i=1}^{n} w_{ij}^{p} \text{dist}(x_i, c_j)^2, \tag{14}$$

where p is a factor which specifies the impact of the weights and $p \varepsilon [0 \ldots \infty]$. If $p > 2$, then the power $1/(p - 1)$ reduces the weight of clusters which are near to the point. If p goes to ∞, then the power goes to 0. This leads to the result that weights tends to $1/k$. If p goes to 1, the power increases the membership weights of points to which the cluster is close. As p goes to 1, the membership tends to 1 for the closest cluster and it tends to 0 for other clusters (same like k-means). Figure 7 shows the application of FCM in MRI of knee.

The FCM algorithm has been effectively used in medical images and has proved useful in producing effective results in the case of bad or corrupted images. It produces rapid and reliable results for MRI images with limited human interaction, but it needs enough experience to apply significantly [59,85–87].

4.3 Expectation Maximization

The Expectation Maximization (EM) method is an iterative process to calculate maximum-likelihood estimation. This algorithm is one of the most popular unsupervised methods which use density estimation of data pixels. In this algorithm, two steps are run iteratively to achieve the results. The first one is the E step which calculates the expectation of likelihood and the second one is the M step which calculates the maximum-likelihood estimation. The expected likelihood is found in the E step and it will be used in the M step to minimize it. The parameter used in the M step will be a seed for the next E step until it achieves some desirable square errors [88–90].

The iteration continues until the stop condition is true which contributes a lot in minimizing mistakes and decreasing execution time. The EM algorithm needs to

initialize the Gaussian mixture model parameters [53,91,92]. The initialization of covariance matrices is done by the identity matrix, and the initialization of C-mean values is done by different centres of Gaussian mixture using *k*-means.

Let $X = \{x_1, x_2, \ldots, x_n\}$ be a data set where $x_i \in R^d$ and k components exist in the mixture model. The probability density of the mixture is

$$f(x) = \sum_{i=1}^{k} \alpha_i p(x|\theta_i), \tag{15}$$

where α_i is the probability of selecting each cluster. In other words, we can say it is the weight of each cluster. Therefore

$$\sum_{i=1}^{k} \alpha_i = 1. \tag{16}$$

The Gaussian mixture distribution parameter is $\theta_i = (\mu_i, \sigma_i)$, and P is the density of the Gaussian distribution:

$$f(x|\mu_i, \sigma_i^2) = \frac{1}{\sqrt{2\pi}\sigma_i} \exp\left[-\frac{(x-\mu_i)^2}{2\sigma_i^2}\right], \quad i = 1, 2, \ldots, N. \tag{17}$$

The parameters will be estimated by maximizing the likelihood. It starts with k numbers of Gaussian to fix a priority and then to look for a local maximum in the first-order conditions [93]. Overall, the EM algorithm can be summarized as follows:

Algorithm:

(1) Evaluation expectancy (E):

$$\alpha_{ij}^{(r+1)} = \alpha^{(r+1)}(i|x_j) = \frac{\alpha_i^r f(x_j|\mu_i^r, (\sigma_i^r)^2)}{f(x_j)}.$$

(2) Maximization step (M): Updating parameters of Gaussian Mixture Model (GMM)

$$\alpha_i^{(r+1)} = \frac{1}{n}\sum_{j=1}^{k} \alpha_{ij}^{(r+1)},$$

$$\mu_i^{(r+1)} = \frac{\sum_{j=1}^{n} x_j \alpha_{ij}^{(r+1)}}{n\ \alpha_i^{(r+1)}},$$

$$(\sigma_i^r)^2 = \frac{\sum_{j=1}^{n} \alpha_{ij}^{(r+1)} (x_j - \mu_i^{(r+1)})(x_j - \mu_i^{(r+1)})^T}{n\, \alpha_i^{(r+1)}}.$$

We stop when $\| \theta^{r+1} - \theta^r \| < \varepsilon$.

Table 1: The estimated values of the expectation maximization algorithm using the Gaussian mixture model

Class number	Weight of GM	Mean	Variance
Class 1	0.1133	0.2801	4.4409e−004
Class 2	0.3096	0.1645	8.8701e−006
Class 3	0.3890	0.2104	6.2457e−004
Class 4	0.1881	0.3339	4.2821e−004

The EM algorithm has been applied in an MRI image and the means and variances for four clusters have been obtained. Table 1 shows the mean and variance for each cluster and Figure 8 shows pixels of each cluster separately.

As can be seen, four images have been extracted from the original image based on EM results. It can help us to separate different tissues from each other.

5. HYBRID METHODS

Some segmentation methods work based on regions like region growing, region merging, etc., while some other methods are based on boundaries like active contour, deformable model, etc. Hybrid methods are based on the ROI and boundary. These methods use both boundary and regional information to segment the images. The results of these methods are rather better than other segmentation approaches applied in medical images. Here we explain graph-cut segmentation methods which present good accuracy in different medical images [94].

5.1 Graph Cut

Some segmentation methods need a number of initial values to start the process like region growing. These methods are known as interactive segmentation methods. These kinds of segmentation methods are becoming more and more popular in solving difficult problems. The graph-cut method tries to separate images into two parts: "object" and "background". User enforces specific constraints for segmentation by selecting some pixels as seed points which are certainly a part of the object and some pixels which belong to the background (Figure 9). Thus, the segmentation method will separate images into two parts by satisfying the constraint enforced by the user [95].

This segmentation method presents a novel interaction approach which is known as the region and boundary detection technique. This method performs segmentation by applying the minimum cut algorithm to find a minimum cut on the graph generated from image pixels [96,97]. Recently, this method has been widely used

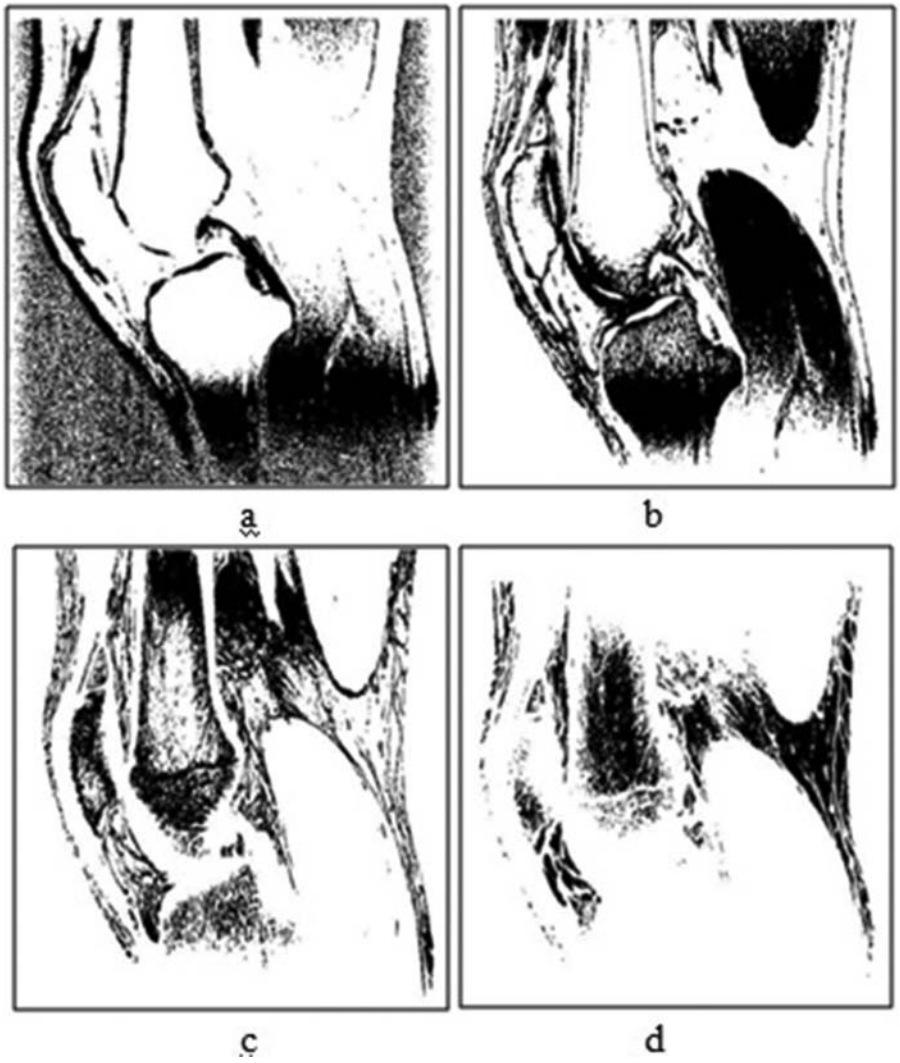

Figure 8: The result of applying EM. (a) Pixels of class 1. (b) Pixels of class 2. (c) Pixels of class 3. (d) Pixels of class 4.

in different areas. Some segmentation methods have been generated based on the graph cut like grab cut [98] and lazy snapping [99].

The advantage of graph-cut methods is presenting an optimum result for segmentation with N dimensions. In addition, it is necessary to define the clear cost function for it. Some recent methods like deformable template, snakes shortest path, ratio regions, etc., have shown optimum results in two-dimensional applications when the segmentation boundary is a one-dimensional curve [95,96,100]. In the declaration of a cost function, boundary and region terms are used. Although some methods have no cost function, graph-cut segmentation can still be managed more consistently using a cost function [12,101].

6. VALIDATION MEASUREMENTS

When we use a segmentation method, it is necessary to compare the results with other methods or other works. Thus, we need some measurement to evaluate the accuracy of segmentation. Here we present some measurements frequently used by researchers. These measurements compare algorithm results with the ground truth labelling. The first one is the Dice Similarity Index (DSI) which quantifies the region overlap between the automatic and manual segmentation [102]:

$$\mathrm{DSI} = 2\frac{|A_A \cap A_G|}{|A_A| + |A_G|}. \tag{18}$$

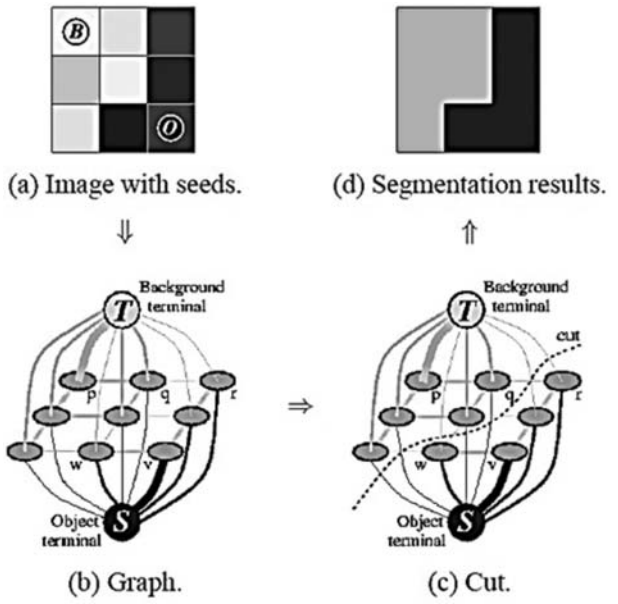

Figure 9: Labelling by graph cut. (a) User selected seed points as the foreground and background. (b) A weighted graph is generated. (c) Minimum cut is calculated. (d) Segmentation results are achieved [96].

The four other measurements are true negative fraction (TNF), false negative fraction (FNF), true positive fraction (TPF), and false positive fraction (FPF) [103]. These measurements are defined as follows:

$$\text{TPF} = \frac{|A_A \cap A_G|}{|A_G|}, \tag{19}$$

$$\text{FPF} = \frac{|A_A - A_G|}{|\overline{A_G}|}, \tag{20}$$

$$\text{TNF} = \frac{|\overline{A_A \cup A_G}|}{|\overline{A_G}|}, \tag{21}$$

$$\text{FNF} = \frac{|A_G - A_A|}{|\overline{A_G}|}, \tag{22}$$

where A_G and A_A indicate the region of ground truth of the foreground (manually) and the region of segmentation of the foreground by the proposed algorithm (automatically), respectively.

7. CONCLUSION

This paper explains a number of current image processing methods which are widely used in medical image analysis. The algorithms and their applications in medical image analysis are presented. Some of them have been applied in MRI images, especially for the knee bone. The description of each method will facilitate in selecting the suitable segmentation method. An appropriate segmentation method can be selected based on different parameters such as the goal of the study, image type, and image characteristics. We categorized these methods in four groups: region-based method, clustering method, classifier method, and hybrid method. Thresholding (global, local, Otsu) and region growing upon which region-based approaches are based are also explained. This category is very sensitive to noise, but they are simple to implement. They do not have good results in MRI without preprocessing but are effective for CT images which have less noise. MRI is more useful than CT imaging for soft tissues. Clustering and classification methods are known as the learning methods. They do not use spatial or shape information. Clustering techniques need training data to start the algorithm. Training data is a time-consuming and difficult task. Among the clustering methods, fuzzy C-mean has shown better accuracy for different medical images. Hybrid methods use the region and boundary properties at the same time to segment the images. The graph-cut method presents optimum results for *N*-dimensional segmentation using a cost function and shows reasonable accuracy. In order to compare segmentation results, different validation methods have been described. Five most popular validation formulae are DSI, TNF, FNF, TPF, and FPF which have been explained to evaluate segmentation results and to compare different methods.

ACKNOWLEDGEMENT

Our deepest thanks to Deanship of Scientific Research at King Saud University, Riyadh, KSA, for their support to conduct this research.

REFERENCES

1. T. Saba, S. Alzorani, and A. Rehman, "Expert system for offline clinical guidance and treatment," *Life Sci. J.*, Vol. 9, no. 4, pp. 2639–58, 2012.
2. A. Norouzi, A. Rahman, M. Shafry, and T. Saba, "Visualization and segmentation," *Int. J. Acad. Res.*, Vol. 4, no. 2, pp. 202–8, 2012.
3. J. Maintz, and M. Viergever, "A survey of medical image registration," *Med. Image Anal.*, Vol. 2, no. 1, pp. 1–36, 1998.
4. T. Saba, and A. Rehman, "Effects of artificially intelligent tools on pattern recognition," *Int. J. Mach. Learn. Cybern.*, Vol. 4, pp. 155–62, 2012.
5. A. Rehman, and T. Saba "Neural network for document image preprocessing," *Artif. Intell. Rev.*, Vol. 4, no. 2, pp. 155–62, 2012.
6. M. S. M. Rahim, A. Rehman, N. Sholihah, F. Kurniawan, and T. Saba, "Region-based features extraction in ear biometrics," *Int. J. Acad. Res.*, Vol. 4, no. 1, pp. 37–42, 2012.
7. S. M. N. K. A. K. Dhara, "Computer-aided detection and analysis of pulmonary nodule from CT images: A survey," *IETE Tech. Rev.*, Vol. 29, no. 4, pp. 265–75, 2012.
8. R. B. Dubey, M. Tech, and H. Madasu, "The brain image segmentation technique and use of diagnostic packages," *Acad. Radiol.*, Vol. 17, no. 5, pp. 658–71, 2010.
9. R. Metter, J. Beutel, and H. Kundel, *Handbook of Medical Imaging*. Washington, DC: SPIE Publications, 2009, pp. 37–45.

10. I. Bankman, T. Nizialek, I. Simon, O. Gatewood, I. Weinberg, and W. Brody, "Segmentation algorithms for detecting microcalcifications in mammograms," *IEEE Trans. Inform. Techn. Biomed*., Vol. 1, no. 2, pp. 141–9, 1997.
11. A. Rehman, and T. Saba, "Features extraction for soccer video semantic analysis: Current achievements and remaining issues," *Artif. Intell. Rev.*, Vol 41, no. 3, pp. 451–61, 2012.
12. A. Rehman, and T. Saba, "Document skew estimation and correction: Analysis of techniques, common problems and possible solutions," *Appl. Artif. Intell.*, Vol. 25, no. 9, pp. 769–87, 2011.
13. G. Saradhi, G. Gopalakrishnan, A. Roy, R. Mullick, R. Manjeshwar, K. Thielemans, and U. Patil, "A framework for automated tumor detection in thoracic FDG pet images using texture-based features," in *Proceedings of the IEEE International Symposium on Digital Object Identifier*, Boston, MA, 2009, pp. 97–100.
14. Z. Zhang, W. Stoecker, and R. Moss, "Border detection on digitized skin tumor images," *IEEE Trans. Med. Imaging*, Vol. 9, no. 11, pp. 1128–43, 2000.
15. U. Kurkure, A. Pednekar, R. Muthupillai, S. Flamm, and I. Kakadiaris, "Localization and segmentation of left ventricle in cardiac cine-MR images," *IEEE Trans. Biomed. Eng.*, Vol. 56, no. 5, pp.1360–70, 2009.
16. F. Castro, C. Pollo, R. Meuli, P. Maeder, O. Cuisenaire, M. Cuadra, J.-G. Villemure, and J.-P. Thiran, "A cross validation study of deep brain stimulation targeting: From experts to atlas-based, segmentation-based and automatic registration algorithms," *IEEE Trans. Med. Imaging*, Vol. 25, no. 11, pp. 1440–50, 2006.
17. J. Rogowska, "Overview and fundamentals of medical image segmentation," in *Handbook of Medical Imaging*, Orlando, FL: Academic Press, 2000, pp. 69–85.
18. T. Saba, A. Rehman, and G. Sulong, "An intelligent approach to image denoising," *J. Theor. Appl. Inf. Technol.*, Vol. 17, no. 1, pp. 32–6, 2010.
19. K. Lim, and A. Pfefferbaum, "Segmentation of MR brain images into cerebrospinal fluid spaces, white and gray matter," *J. Comput. Assist. Tomogr.*, Vol. 13, no. 4, pp. 588–93, 1989.
20. F. Lucas-Quesada, U. Sinha, and S. Sinha, "Segmentation strategies for breast tumors from dynamic MR images," *J. Magn. Reson. Imaging*, Vol. 6, no. 5, pp. 753–63, 1996.
21. E. Davies, *Machine Vision: Theory, Algorithms, Practicalities*. San Francisco, CA: Morgan Kaufmann, 2005.
22. M. Sonka, V. Hlavac, and R. Boyle, *Image Processing: Analysis and Machine Vision*. Pacific Grove, CA: PWS Publishing, pp. 123–33, 1999.
23. R. Dalvi, R. Abugharbieh, D. Wilson, and D. Wilson, "Multi-contrast MR for enhanced bone imaging and segmentation," *Conf. Proc. IEEE Eng. Med. Biol. Soc.*, Vol. 2007, pp. 5620–3, 2007.
24. M. S. Swanson, J. W. Prescott, T. M. Best, K. Powell, R. D. Jackson, F. Haq, and M. N. Gurcan, "Semi-automated segmentation to assess the lateral meniscus in normal and osteoarthritic knees," *Osteoarthritis cartilage*, Vol. 18, pp. 344–53, 2010.
25. A. E. Rad, M. S. M. Rahim, A. Rehman, A. Altameem, and T. Saba, "Evaluation of current dental radiographs segmentation approaches in computer-aided applications," *IETE Tech. Rev.*, Vol. 30, no. 3, pp. 210–22, 2013.
26. P. Sahoo, S. Soltani, and A. Wong, "Survey of thresholding techniques," *Comp. Vis. Graph. Image Proc.*, Vol. 41, no. 2, pp. 233–60, 1988.
27. A. Rehman, and T. Saba, "Performance analysis of segmentation approach for cursive handwritten word recognition on benchmark database," *Digit. Signal Process.*, Vol. 21, no. 3, pp. 486–90, 2011.
28. J. Weszka, "A survey of threshold selection techniques," *Comp. Graph. Image Proc.*, Vol. 7, pp. 259–65, 1978.
29. A. Rehman, and D. Mohamad, "A simple segmentation approach for unconstrained cursive handwritten words in conjunction of neural network," *Int. J. Image Process.*, Vol. 2. no. 3, pp. 29–35, 2008.
30. A. Norouzi, T. Saba, M. S. M. Shafry, and A. Rehman, "Visualization and segmentation of 3D Bone from CT images," *Int. J. Acad. Res.*, Vol. 4, no. 2, pp.202–8, 2012.
31. D. L. Pham, C. Xu, and J. L. Prince, "A survey of current methods in medical image segmentation," *Ann. Rev. Biomed. Eng.*, Vol. 2, pp. 315–37, 1998.
32. C. Leea, S. Huha, T. A. Ketter, and M. Unserc, "Unsupervised connectivity-based thresholding segmentation of midsagittal brain MR images," *Comp. Biol. Med.*, Vol. 28, no. 3, pp. 309–38, 1998.
33. J. Zhang, C. Yan, C. Chui, and S. Ong, "Fast segmentation of bone in CT images using 3D adaptive thresholding," *Comput. Biol. Med.*, Vol. 40, no. 2, pp. 231–36, 2010.
34. R. S. A. V. K. V. Shrimali, "Current trends in segmentation of medical ultrasound B-mode images: A review," *IETE Tech. Rev.*, Vol. 1, no. 8–17, pp. 26, 2009.
35. T. J. U. C. T. Ahsan, "Facial expression recognition using local transitional pattern on Gabor filtered facial images," *IETE Tech. Rev.*, Vol. 30, no. 1, pp. 47–52, 2013.
36. A. Paul, K. Bharanitharan, and J. Wu, "Algorithm and architecture for adaptive motion estimation in video processing," *IETE Tech. Rev.*, Vol. 30, no. 1, pp. 24–30, 2013.
37. K. Sun, "Development of segmentation methods for vascular angiogram," *IETE Tech. Rev.*, Vol. 28, no. 5, pp. 392–9, 2011.
38. N. Nguyen, D. Laurendeau, and A. Branzan-Albu, "A new segmentation method for MRI images of the shoulder joint," in *Fourth Canadian IEEE Conference on Computer and Robot Vision (CRV'07)*, Montreal, May 28–30, pp. 329–38, 2007.
39. R. Haralick and L. Shapiro, "Image segmentation techniques," *Comp. Vis. Graph. Image Proc*., Vol. 26, pp. 100–32, 1985.
40. R. Gonzalez, and R. Woods, *Digital Image Processing*. Englewood Cliffs, NJ: Prentice Hall, pp: 612–7, 2002.
41. M. Kallergi, K. Woodsa, L. Clarkea, and W. Qiana, "Image segmentation in digital mammography: Comparison of local thresholding and region growing algorithms," *Comp. Med. Imag. Graph.*, Vol. 16, no. 5, pp. 323–31, 1992.
42. R. Adams, and L. Bischof, "Seeded region growing," *IEEE Trans. Pattern Anal. Mach. Intell.*, Vol. 16, no. 6. pp. 641–7, 1994.
43. J. Fan, G. Zeng, M. Body, and M. Hacid, "Seeded region growing: An extensive and comparative study," *Pattern Recog. Lett.*, Vol. 26, no. 8, pp. 1139–56, 2005.
44. J. Freixenet, D. Raba, A. Oliver, and J. Espunya, "Breast profile segmentation based on the region growing approach," *Int. Cong. Ser.*, Vol. 1281, pp. 1281–397, 2005.
45. G. Hu, and Mageras, "Survey of recent volumetric medical image segmentation techniques," *Biomedical Engineering*, Vukovar, Crotia: In-Tech, pp. 321–6, 2009.
46. G. Rabottino, A. Mencattini, M. Salmeri, F. Caselli, and R. Lojacono, "Performance evaluation of a region growing procedure for mammographic breast," *Comp. Stand. Inter.*, Vol. 33, no. 2, pp. 128–35, 2011.
47. Z. Huo, M. Giger, C. Vyborny, and U. Bick, "Analysis of speculation in the computerized classification of mammographic masses," *Med. Phys.*, Vol. 22, no. 10, pp. 1569–79, 1965.
48. S. Umbaugh, *Computer Vision and Image Processing: A Practical Approach Using CVIPTools*. Upper Saddle, NJ: Prentice Hall PTR, pp. 1–40, 1997.
49. A. Olivera, J. Jordi Freixeneta, and J. Joan Martía, "A review of automatic mass detection and segmentation in mammographic images," *Med. Image Anal.*, Vol. 14, no. 2, pp. 87–110, 2010.

50. C. M. Bishop, *Pattern Recognition and Machine Learning*. New York: Springer, pp. 1−5, 2006.
51. W. Gibson, *Pattern Recognition*. Berkley: Berkley Press, pp. 74−89, 2005.
52. S. Theodoridis, A. Pikrakis, K. Koutroumbas, and D. Cavouras, *Introduction to Pattern Recognition: A Matlab Approach*. Burlington, VT: Academic Press, 2010.
53. W. Wells, W. Grimson, R. Kikins, and F. Jolesz, "Adaptive segmentation of MRI data," *IEEE Trans. Med. Imag.*, Vol. 15, no. 4, pp. 429−42, 1996.
54. J. Mantas, "Methodologies in pattern recognition and image analysis—A brief survey," *Pattern Recog.*, Vol. 22, no. 1, pp. 1−6, 1987.
55. E. S. El-Dahshan, T. Hosny, and A. M. Salem, "Hybrid intelligent techniques for MRI brain images classification," *Digit. Signal Process.*, Vol. 20, no. 2, pp. 433−41, 2010.
56. K. Murphya, B. van Ginnekena, A. Schilhama, and B. Hoopb, "A large-scale evaluation of automatic pulmonary nodule detection in chest CT using local image features and k-nearest-neighbour classification," *Med. Image Anal.*, Vol. 13, no. 5, pp. 757−70, 2009.
57. H. Yan, J. Mao, Y. Zhu, and B. Chen, "Magnetic resonance image segmentation using optimized nearest neighbor classifiers," *IEEE Proc. ICIP*, Vol. 3, pp. 49−52, 1994.
58. J. Bezdek, "Computing with uncertainty," *IEEE Commun. Mag.*, Vol. 30, no. 2, pp. 24−36, 1992.
59. L. Clarke, R. P. Velthuizen, S. Phuphanich, J. Schellenberg, J. Arrington, and M. Silbiger, "MRI: Stability of three supervised segmentation techniques," *Magn. Reson. Imag.*, Vol. 11, no. 1, pp. 95−106, 1993.
60. S. Hua, and P. Shao, "Improved nearest neighbor interpolators based on confidence region in medical image registration," *Biomed. Signal Process. Control*, Vol. 7, no. 5, pp. 525−36, 2012.
61. J. M. Keller, M. R. Gray, and J. A. Givene, "A fuzzy K-nearest neighbor algorithm," *IEEE Trans. Syst. Man Cybern.*, Vol. SMC-15, no. 4, pp. 580−5, 1985.
62. I. Myung, "Tutorial on maximum likelihood estimation," *J. Math. Psychol.*, Vol. 47, no. 1, pp. 90−100, 2003.
63. J. Xie, and H. Tsui, "Image segmentation based on maximum-likelihood estimation and optimum entropy-distribution (MLE−OED)," *Pattern Recog. Lett.* Vol. 15, no. 10, pp. 1133−41, 2004.
64. S. Choi, and R. Wette, "Maximum likelihood estimation of the parameters of the gamma distribution and their bias," *Technometrics*, Vol. 11, no. 4, pp. 683−90, 1969.
65. K. Chuang, M. Jan, J. Wu, and J. Lu, "A maximum likelihood expectation maximization," *Comput. Med. Imag. Graph.*, Vol. 29, no. 7, pp. 571−8, 2005.
66. P. Rahmatia, A. Adler, and G. Hamarneh, "Mammography segmentation with maximum likelihood active contours," *Med. Image Anal.*, Vol. 16, no. 6, pp. 20, 2012.
67. A. Sarti, C. Corsi, E. Mazzini, and C. Lamberti, "Maximum likelihood segmentation of ultrasound images with rayleigh distribution," *IEEE Trans. Ultrason. Ferro. Freq. Contr.*, Vol. 52, no. 6, pp. 947−60, 2005.
68. J. Schalkoff, *Pattern Recognition: Statistical, Structural and Neural Approach*. New York: Wiley, pp. 109−27, 1992.
69. E. Alpaydm, *Introduction to Machine Learning*. London: MIT Press, pp. 143−63, 2004.
70. F. Gonzalez, and E. Romero, *Biomedical Image Analysis and Machine Learning Technologies: Applications and Techniques*. Medical Information Science Reference, USA, pp. 1−27, 2009.
71. F. Camastra, and A. Vinciarelli, *Machine Learning for Audio, Image and Video Analysis: Theory and Applications*. London: Springer, pp. 117−32, 2010.
72. S. Marsland, *Machine Learning: An Algorithmic Perspective*. Cambridge, UK: Chapman and Hall/CRC, pp. 195−220, 2009.
73. S. Redmond, and C. Heneghan, "A method for initialising the K-means clustering algorithm using kd-trees," *Pattern Recog. Lett.*, Vol. 28, no. 8, pp. 965−73, 2007.
74. M. Celebi, H. Kingravi, and P. Vela, "A comparative study of efficient initialization methods for the k-means clustering algorithm," *Expert Syst. Appl.*, Vol. 28, no. 8, pp. 11, 2012.
75. L. Juang, and M. Wu, "MRI brain lesion image detection based on color-converted K-means," *Measurement*, Vol. 43, no. 7, pp. 941−9, 2010.
76. M. Yan, P. Philadelphia, and J. Karp, "Segmentation of 3D brain MR using an adaptive K-means clustering algorithm," in *Proceedings of the Nuclear Science Symposium and Medical Imaging Conference*, Norfolk, VA, pp. 1529−33, 1994.
77. G. Sulong, T. Saba, A. Rehman, and Saparudin. "A new scars removal technique of fingerprint images," in *Proceedings of the IEEE International Conference on Instrumentation Communication, Information Technology and Biomedical Engineering* (*ICICI-BME*), Bandung, Indonesia, 2009, pp. 31−5.
78. K. Meethongjan, D. Mohamad, A. Rehman, A. Altameem, and T. Saba, "An intelligent fused approach for face recognition," *J. Intell. Syst.*, Vol. 22, no. 1, pp. 71−80, 2013.
79. J. Wanga, J. Kongb, Y. Lub, M. Qib, and B. Zhanga, "A modified FCM algorithm for MRI brain image segmentation using both local and non-local spatial constraints," *Comput. Med. Imag. Graph.*, Vol. 32, no. 8, pp. 685−98, 2008.
80. M. Brandt, T. Bohan, L. Kramer, and J. Fletcher, "Estimation of CSF, white matter and gray matter volumes in hydrocephalic children using fuzzy clustering of MR images," *Comput. Med. Imag. Graph.*, Vol. 18, no. 1, pp. 25−34, 1994.
81. M. Ahmed, S. Yamany, N. Mohamed, and A. A. Farag, "A modified fuzzy c-means algorithm for bias field estimation and segmentation of MRI data," *IEEE Trans. Med. Imag.*, Vol. 21, no. 3, pp. 193−9, 2002.
82. M. Yanga, Y. Hua, K. C. Lin, and C. C. Linc, "Segmentation techniques for tissue differentiation in MRI of Ophthalmology using fuzzy clustering algorithms," *Magn. Reson. Imag.*, Vol. 21, no. 3, pp. 173−9, 2002.
83. X. Xie, and G. Beni, "Validity measure for fuzzy clustering," *IEEE Trans. Pattern Anal. Mach. Intell.*, Vol. 13, no. 8, pp. 841−6, 1991.
84. X. Wang, Y. Wang, and L. Wang, "Improving fuzzy c-means clustering based on feature-weight learning," *Pattern Recog. Lett.*, Vol. 13, no. 8, pp. 1123−32, 2004.
85. Z. Ji, Y. Xia, Q. Chen, and Q. Sun, "Fuzzy c-means clustering with weighted image patch for image segmentation," *Appl. Soft Comput.*, Vol. 12, no. 6, pp. 1659−67, 2010.
86. K. Chuang, H. Tzeng, and J. W. S Chen, "Fuzzy c-means clustering with spatial information for image segmentation," *Comput. Med. Imag. Graph.*, Vol. 30, no. 1, pp. 9−15, 2006.
87. M. Yang, Y. Hu, K. Lin, and C. Lin, "Segmentation techniques for tissue differentiation in MRI of ophthalmology using fuzzy clustering algorithms," *Magn. Reson. Imag.*, Vol. 8, no. 6, pp. 173−9, 2002.
88. K. Revathy, and V. Roshni, "Applying EM algorithm for segmentation of textured images," in *Proceedings of the World Congress on Engineering*, London, 2007.
89. C. Carson, and H. Greenspan, "Blobworld: Image segmentation using expectation-maximization and its application to image querying," *IEEE Trans. Pattern Anal. Mach. Intell.*, Vol. 24, no. 8, pp. 1026−38, 2002.
90. H. Chen, X. Lei, and D. Yao, "An improved ordered subsets expectation maximization positron emission computerized tomography reconstruction," *Comput. Biol. Med.*, Vol. 37, no. 12, pp. 1780−5, 2007.

91. Z. K. Huang, "Unsupervised image segmentation using EM algorithm by histogram," *Lect. Notes Comput. Sci.*, Vol. 4681, pp. 1275–82, 2007.
92. R. Luis-García, C. Westin, and C. Alberola-López, "Gaussian mixtures on tensor fields for segmentation: Applications to medical imaging," *Comput. Med. Imag. Graph.*, Vol. 35, no. 1, pp. 16–30, 2011.
93. M. Mahjoub, and K. Kalti, "Image segmentation by adaptive distance based on EM algorithm," *Int. J. Adv. Comput. Sci. Appl.*, pp. 19–25, 2011.[CE: Volume missing]
94. S. Y. Ababneh, J. W. Prescott, and M. N. Gurcan, "Automatic graph-cut based segmentation of bones from knee magnetic resonance images for osteoarthritis research," *Med. Image Anal.*, Vol. 15, no. 4, pp. 438–48, 2011.
95. Y. Booykov, and G. Funka-Lea, "Graph cuts and efficient N-D image segmentation," *Int. J. Comput. Vision*, Vol. 70, no. 2, pp. 109–31, 2006.
96. Y. Boykov, and M. Jolly, "Interactive graph cuts for optimal boundary & region segmentation of objects in N-D images," in *Proceedings of International Conference on Computer Vision*, Vancouver, Canada, pp. 105–12, 2001.
97. Y. Boykov, O. Veksler, and R. Zabih, "Fast approximate energy minimization via graph cuts," *IEEE Trans. Pattern Anal. Mach. Intell.*, Vol. 23, no. 11, pp. 1222–39, 2001.
98. C. Rother, V. Kolmogorov, and A. Blake, "GrabCut interactive foreground extraction using iterated graph cuts," *ACM Trans. Graph. (TOG) – Proc. ACM SIGGRAPH*, Vol. 3, no. 4, pp. 309–41, 2004.
99. Y. Li, J. Sun, C. Tang, and H.-Y. Shum, "Lazy snapping," *SIGGRAPH (ACM Trans. Graph.)*, Vol. 23, no. 3, pp. 303–8, 2004.
100. Y. Boykov, and G. Funka-lea, "Graph cuts and efficient N-D image segmentation," *Int. J. Comput. Vision*, Vol. 70, no. 2, pp. 109–31, 2006.
101. Y. Boykov, O. Veksler, and R. Zabih, "Markov random fields with efficient approximations," in *IEEE Conference on Computer Vision and Pattern Recognition*, Santa Barbara, 23–25 Jun 1998, pp. 648–55, 1998.
102. L. Dice, "Measure of the amount of ecologic association between species," *Ecology*, Vol. 26, pp. 297–302, 1945.
103. B. Peng, L. Zhang, and J. Yang, "Iterated graph cuts for image segmentation," *Lect. Notes Comput. Sci.*, Vol. 5995, pp. 677–86, 2010.

Authors

Alireza Norouzi received his BE degree in computer science from Yazd University, Iran, in 2003 and master's degree in software engineering from Islamic Azad University, Iran, in 2006. Currently, he is pursing PhD from University Technology Malaysia (UTM), Malaysia, and his areas of interest are digital image processing, medical image processing, and computer vision.

E-mail: tsaba@pscw.psu.edu.sa

Mohd Shafry Mohd Rahim received his BSc and MSc degrees in computer science from University Technology Malaysia (UTM) in 1999 and 2002, respectively, and PhD degree in computer science from University Putra Malaysia (UPM). Currently, he is an associate professor in the Faculty of Computing, UTM, and head of ViCubeLab, K-Economy Research Alliance. His research interests include computer graphics, visualization, spatial modelling, image processing, and geographical information systems.

E-mail: tsaba@pscw.psu.edu.sa

Dr Ayman Altameem is vice dean in the College of Applied Studies and Community Services, King Saud University, Riyadh, KSA. He received his PhD degree in information technology and computing from the University of Bradford, Bradford, UK, and MSc degree in information systems and computing from London South Bank University, London, UK. His keen research interests are E-commerce, information processing, and artificial intelligence.

E-mail: tsaba@pscw.psu.edu.sa

Dr Tanzila Saba earned her PhD degree from the Faculty of Computing, Universiti Teknologi Malaysia, Malaysia, in 2012. Her field of specialization is document information management and security. She is an eminent researcher in the Image Processing Research Group and was selected for Marquis Who's Who 2012 award due to her excellent research achievements round the globe. She has published more than 30 papers in high-impact-factor journals. Currently, she is an assistant professor in the College of Computer and Information Sciences, Prince Sultan University, Riyadh, KSA. **E-mail:** tanzilasaba@yahoo.com

E-mail: tsaba@pscw.psu.edu.sa

Abdolvahab Ehsani Rad received his BE degree in computer engineering with the major of software from Islamic Azad University, Iran, in 2006 and MTech degree from the University of Mysore, India, in 2010. Presently, he is pursuing his PhD from Universiti Teknologi Malaysia (UTM), Malaysia. His research interests include digital image processing, medical image processing, and computer vision.

E-mail: tsaba@pscw.psu.edu.sa

Dr. Amjad Rehman is an assistant prof. in MIS department CBA, Salman bin Abdul Aziz University, Alkharj, KSA. He received his PhD from Faculty of Computing Universiti Teknologi, Malaysia with specialization in forensic documents analysis and information security. His keen interests are in image processing and pattern recognition. He is an author of more than 50 indexed journal papers and is a member of IEEE.

E-mail: ar.khan@sau.edu.sa

Dr Mueen Uddin is a Post-Doctoral Research Fellow at the International Islamic University, Malaysia. He earned his PhD degree from Universiti Teknologi Malaysia (UTM) in 2012. His research interests include green IT, energy efficient data centres, green metrics, global warming effects, virtualization, cloud computing, digital content protection and deep packet inspection, intrusion detection and prevention systems, and MANET routing protocols. Dr Mueen earned his BS and MS degrees in computer science from Isra University Pakistan with specialization in information networks. He has published more than 35 international journal papers in high-impact-factor journals.

E-mail: tsaba@pscw.psu.edu.sa

DOI: 10.1080/02564602.2014.906861;